Fire and Materials

WILEY

RESEARCH ARTICLE OPEN ACCESS

Experimental and Numerical Investigation of Cedar Façade Flame Spread With Respect to Sidewall

Xukun Sun[1,2,3] | Hideki Yoshioka[3] | Takafumi Noguchi[3] | Yuhei Nishio[4] | Manabu Kanematsu[5] | Biao Zhou[6] | Mingwei Xu[1]

[1]School of Safety Engineering, Beijing Institute of Petrochemical Technology, Beijing, China | [2]Beijing Academy of Safety Engineering and Technology, Beijing, China | [3]Department of Architecture, Faculty of Engineering, The University of Tokyo, Tokyo, Japan | [4]Department of Fire Engineering, Building Research Institute, Tsukuba, Japan | [5]Department of Architecture, Faculty of Science and Technology, Tokyo University of Science, Chiba, Japan | [6]School of Emergency Management and Safety Engineering, China University of Mining and Technology, Beijing, China

Correspondence: Hideki Yoshioka (yoshioka@arch1.t.u-tokyo.ac.jp)

Received: 22 August 2025 | **Revised:** 12 October 2025 | **Accepted:** 29 October 2025

Keywords: accelerated weathering | façade fire | fire retardant | large eddy simulation (LES) | large-scale test | sidewall effect

ABSTRACT

In response to growing energy conservation and carbon neutrality efforts, façade systems incorporating wooden materials have attracted increasing attention, which in turn raises concerns about their combustibility. This study presents a combined experimental and numerical investigation of flame spread along cedar façades. Experimental results reveal that for untreated cedar, once flames penetrate cedar façades, the vent layer flame spread plays a crucial role in the secondary intensification of façade fire spread. For fire-retardant-treated cedar, the enhanced char-forming capability significantly mitigates façade flame spread and limits burnt area, contributing to maintaining the structural integrity of façade regions beyond direct flame exposure. Although the leaching effect of accelerated weathering reduces fire retardant retention, it causes only minor deterioration in cedar fire performance. The numerical modeling, validated against measured temperatures, shows good agreement, although it underestimates the second temperature peak due to simplifications of flame spread inside the vent layer. Furthermore, the impact of a single sidewall on cedar façade fire risk is clarified using the validated modeling, which indicates that the sidewall effect significantly accelerates flame spread compared to the no-sidewall condition. Moreover, the fire-risky sidewall distance tends to increase due to the additional HRR generated by cedar façade combustion.

1 | Introduction

With the appeal of carbon neutral and sustainable development, some façade systems are increasingly installed to optimize the energy conservation of modern buildings. In this case, wood receives attention as a façade material because of its superiorities in recyclability, low environmental impact, aesthetic features, and constructive properties [1, 2], as shown in Figure 1.

However, several infamous façade fire incidents, such as the Grenfell Tower fire [3] and the Shanghai apartment fire [4], have raised people's attention regarding the fire safety of façade systems, which are essentially caused by the combustibility of façade materials [5]. Generally, the combustibility of wood is also one of the main challenges limiting the wide use of wooden façades. Nevertheless, with the advancement of fire retardant and auto-extinguishing systems, wooden façades become the proper choice in Denmark, Sweden, Finland, etc. [6, 7] for interior and exterior applications when meeting the required reaction to fire classification [1].

Numerous studies regarding wooden façade fires have been conducted through experimental and numerical approaches. Hakkarainen et al. [7] and Nishio et al. [8] evaluate the reaction-to-fire performance of wooden façades by SP Fire 105 and JIS A 1310, finding that fire retardant is crucial in delaying or even

FIGURE 1 | Wooden façade in modern buildings.

halting flame spread. Ostman et al. [6] also proceeded with the wooden façade using the SP Fire 105 test and further emphasized the importance of weather durability of fire retardant treatment and fire stop. With respect to the numerical approach, Duny et al. [9] conducted a parametric analysis of simulations according to the façade tests of varied wood varieties. Giraldo et al. [1] investigated the influence of horizontal projection on flame spread along wooden façades. Zhou et al. [10] evaluated the impact of wood properties on façade fire performance. However, a comprehensive understanding of flame spread along fire-retardant-treated or weathered wooden façades is still required, and knowledge of the sidewall effect on wooden façade fires is deficient.

This study experimentally investigates the reaction-to-fire performance of large-scale cedar façades, both treated and untreated with fire retardant, and with or without accelerated weathering, accompanied by a discussion of the underlying mechanisms. Based on experiment-validated modeling, the flame spread of cedar façades involving a single sidewall is analyzed, with particular focus on the influence of cedar combustion on the fire-risky sidewall distance.

2 | Experimental and Numerical Configurations

2.1 | Experimental Facilities

The large-scale façade fire test, conducted following the JIS A 1310 standard [11], involves the installation of cedar along the façade and provides valuable insights into large-scale flame spread along cedar surfaces. During the experiments, the uncertainty and repeatability of the facilities, testing environment, and material conditions are ensured by compliance with JIS C 1602 [12], JIS Z 8703 [13], and JIS A 1326 [14], respectively. The dimensions of JIS A 1310 are shown in Figure 2a, including the chamber, opening, and burner (heat release rate [HRR] of 900 kW). During the experiment, the ignition and combustion of the cedar façade are initiated by the outflow flame generated by the combustion chamber. Figure 2b provides details of the cedar façade installation. The entire cedar façade comprises multiple cedar panels assembled horizontally using tongue and grooved joints along the panel edges. The panels are affixed to furring, creating a vent layer between the cedar façade and the substrate. Although the vent layer surrounding the opening edges (as shown in the structural diagram of Figure 2b) is obstructed by the ceramic fiber blanket, the flame is expected to penetrate into the vent layer through the front surface of the cedar façade during the experiment. Temperature distribution along the centerline of the cedar façade is measured using a series of K-type thermocouples positioned at 500, 900, 1500, 2000, and 2500 mm above the opening. Additionally, thermocouples inside the vent layer are mounted vertically above both the right and left edges of the opening, positioned at the same heights as those installed along the cedar façade surface. The uncertainties of these K-type thermocouples are ±2.5°C for temperatures below 333°C and ±0.75% for temperatures between 333°C and 1200°C.

Three types of cedar specimens are tested: (1) No fire retardant or accelerated weathering; (2) fire retardant but no accelerated weathering; and (3) fire retardant and accelerated weathering, as indicated in Figure 2c. Specimens 1, 2, and 3 are employed to represent the different treatments of cedar. Fire-retardant cedar is treated with phosphoric acid-based amino using high-pressure impregnation techniques. This treatment results in the fire retardant retention of $121 \pm 7\,kg/m^3$ for the cedar specimens. The coating of alkyd is additionally treated on fire-retardant cedar to improve the weather resistance. Then, specimen 3 is subjected to accelerated weathering tests following the JIS A 1326 [14], involving a total of 180 cycles, which is equivalent to approximately 3 years of natural weathering. As shown in Figure 3, each cycle comprises a 1.5-h drying process and a subsequent 2-h watering process. During the drying process, the surface temperature of the cedar specimens is maintained at 80°C ± 3°C, while in the watering process, the surface temperature is reduced with a water supply flow rate of $1\,L/(m^2 \cdot min)$. All cedar specimens are dried for 24 h at 80°C ± 3°C, followed by a two-week curing period at 23°C and 50% relative humidity to ensure consistent conditions prior to testing.

2.2 | Numerical Setup

In accordance with the cedar façade fire test, the computational domain and mesh slice are shown in Figure 4. The red dashed box highlights a local zoomed-in region to illustrate the façade mesh configuration. The mesh configuration employs a baseline mesh of 10 cm and a refined mesh of 2.5 cm. The 2.5 cm mesh covers the flame region, encompassing both the chamber and the area adjacent to the façade. The internal domain aligns with the chamber dimensions, and the external domain is $L \times W \times H = 4\,m \times 4\,m \times 5\,m$. Consistent with experimental

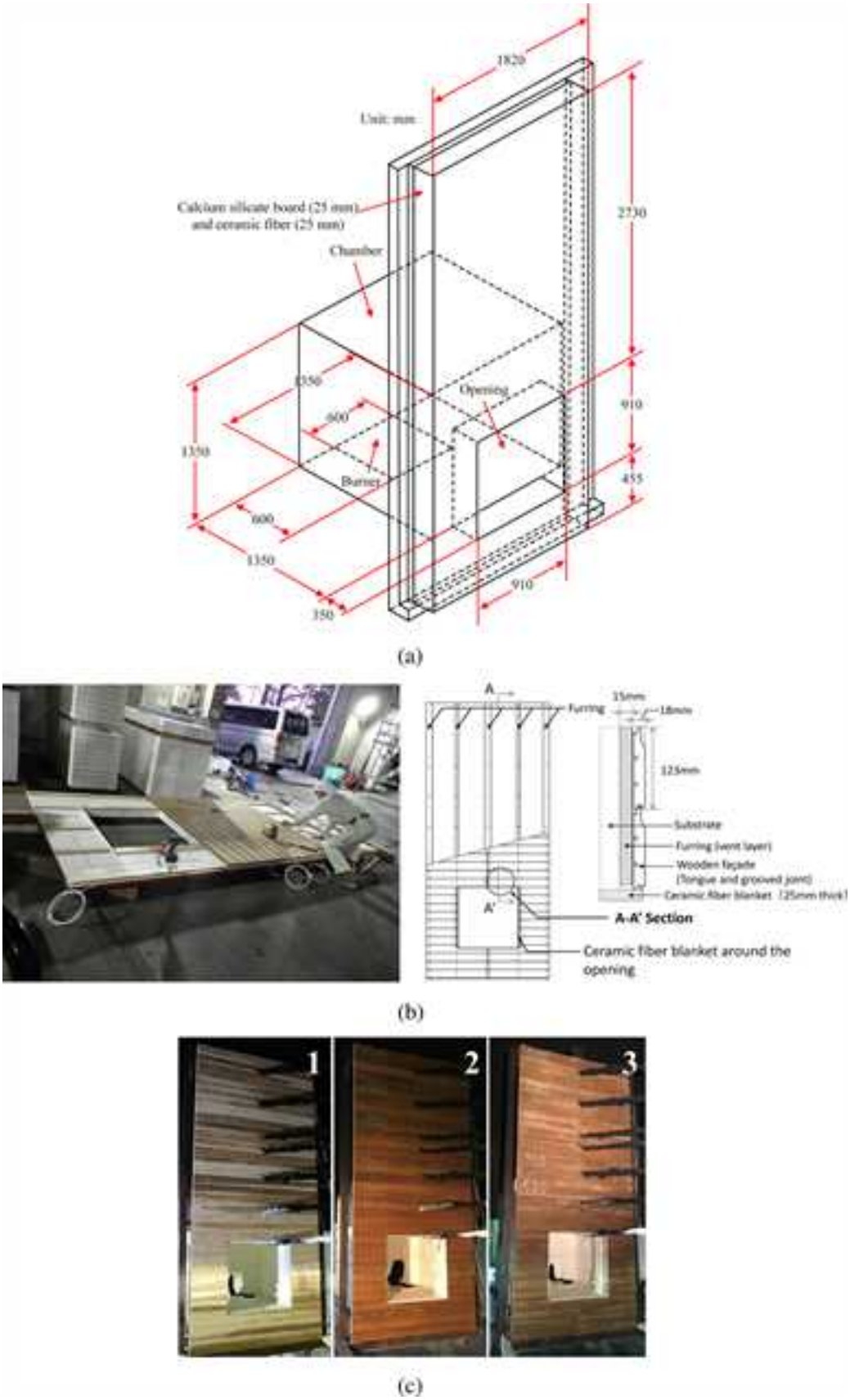

FIGURE 2 | Experimental layout. (a) Dimensions of JIS A 1310. (b) Installation of cedar façade. (c) Appearance of specimens 1. No fire retardant or accelerated weathering, 2. fire retardant but no accelerated weathering, and 3. fire retardant and accelerated weathering.

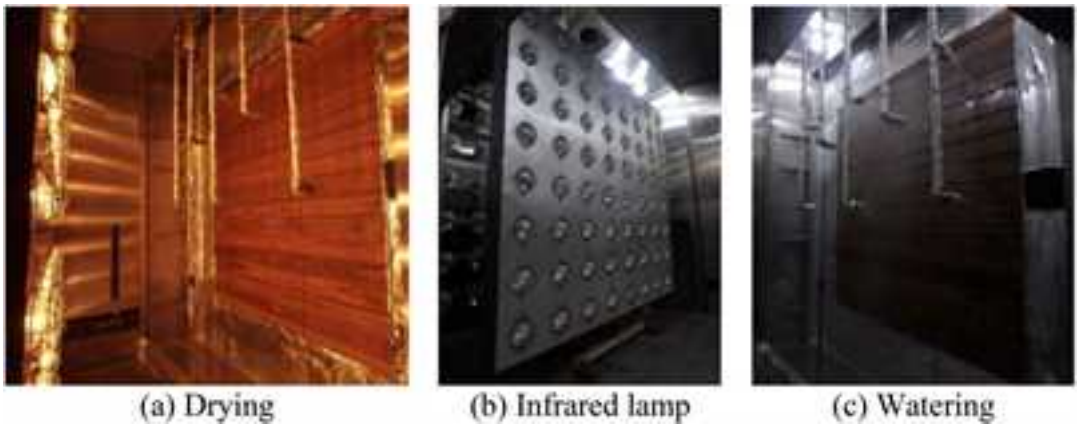

FIGURE 3 | Accelerated weathering test.

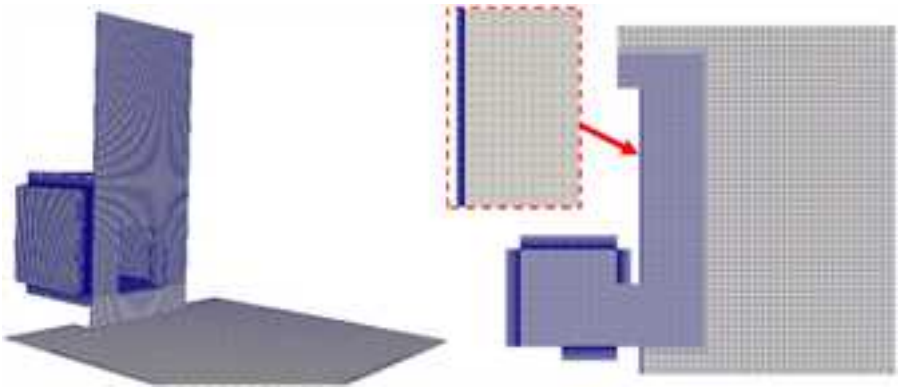

FIGURE 4 | Computational domain and mesh configuration.

TABLE 1 | Mesh information of cedar façade modeling.

Region	Location	Thickness (cm)	Layer	Size (cm)	Cell number
Fluid	Flame (inside the chamber and adjacent to the façade)	/	/	2.5	63.6×10^4
	Non-flame	/	/	10	
Solid	Chamber wall	20	100	/	169.44×10^4
	Façade wall	1.8	180	/	34.67×10^4

conditions, the test duration is set to 1200 s, with a burner HRR of 900 kW.

Table 1 presents the detailed mesh information. Aiming to capture the flame spread along the cedar façade, both the chamber and façade are modeled with material/solid regions to account for heat conduction and combustion. The 20 cm thick solid regions are extended perpendicularly from the chamber's inner surface to model the chamber walls and are treated as non-combustible materials by defining an extremely large activation energy. Regarding the cedar façade, its thickness is set at 1.8 cm, with material properties provided by Koshii & Co. Ltd [10] as shown in Table 2. Here, the vent layer between the cedar façade and the substrate cannot be modeled directly due to its extremely small size relative to the overall scale and is instead considered through a convective heat transfer boundary condition. The chamber and façade are considered as walls with heat transfer boundaries between the fluid and solid regions. In addition, a sub-grid thermal diffusivity model [15] is applied to the façade to correct the convective heat flux. The floor is defined as an adiabatic boundary, while the burner corresponds to the prescribed propane mass flow rate with 900 kW HRR. The boundaries at the top of the computational domain and its surroundings are specified as open boundaries.

The open-source computational fluid dynamics (CFD) solver of FireFOAM [16] is utilized to simulate the façade flame spread, which is based on the finite volume method (FVM) with the turbulence modeling of large eddy simulation (LES). In this case, the sub-grid scale (SGS) turbulence, combustion, and radiation are solved by the one-equation eddy viscosity model, modified eddy dissipation concept (EDC) model, and discrete ordinate method (DOM), respectively. A detailed description of sub-models can be found in [4], as well as the mesh sensitivity analysis. Building on this, the cedar combustion is further considered by coupling the one-dimensional pyrolysis [17] and mass transfer boundary.

TABLE 2 | Material properties for cedar façade.

	Property	Unit	Value
Cedar	Density	kg/m^3	500.3
	Heat capacity	J/(kg·K)	1266
	Conductivity	W/(m·K)	0.11
	Emissivity		0.17
Char	Density	kg/m^3	52.3
	Heat capacity	J/(kg·K)	800
	Conductivity	W/(m·K)	0.16
	Emissivity		0.85
Reaction	Pre-exponential factor	s^{-1}	2.75×10^7
	Activation energy	J/mol	1.37×10^5
	Reaction order		3.02
	Heat of pyrolysis	J/kg	2.92×10^5

3 | Results and Discussion

3.1 | Results of JIS A 1310 Façade Test

The results of large-scale façade fire tests with specimens 1, 2, and 3 are presented in Figure 5, including the temperature along the cedar façade and inside the vent layer. In Figure 5a, the temperature along the façade surface of specimen 1 exhibits intensified flame spread compared to the calibration test (non-combustible façade). This enhancement becomes significant with the elevation of height. Note that the initial temperature peaks become pronounced outside the visible flame (height > 900 mm), attributed to the rapid cedar surface combustion, but diminish gradually due to char layer formation. For heights ≤ 1500 mm, the direct impact of outflow flames leads to rapid burnout of the cedar façade, resulting in a monotonic temperature decrease without a secondary temperature peak. However, for heights > 1500 mm, cedar combustion is slower. In this scenario, the flame spreads inside the vent layer as the lower part of the cedar façade burns away, and the higher part of the cedar façade is subjected to flame heating from both the front and back. This leads to accelerated combustion with a re-increased surface temperature. Additionally, according to Figure 5b, the vent layer temperature at 2000 and 2500 mm initiates increases after 800 s, which aligns with the trend of surface temperature increase in Figure 5a, indicating that the flame spread inside the vent layer is critical to the secondary peak/combustion along the façade surface of specimen 1.

For the fire-retardant cedar of specimens 2 and 3, their temperature development remains more stable, showing no intense flame spread. In these cases, the two-peaks phenomenon is absent, and the façade temperature gradually approaches the results of calibration tests. Notably, specimen 3, subjected to accelerated weathering, exhibits relatively higher temperatures compared to specimen 2, indicating an elevated fire risk. This can be attributed to the leaching effect caused by accelerated weathering, which diminishes the fire-retardant retention in the specimens [18], thereby reducing their fire performance. In Figure 5b, the vent layer temperatures at different elevations increase sequentially for specimen 1, indicating that continuous flame spread compromises the mechanical properties of cedar. Consequently, the vent layer is directly affected by outflow flames, leading to progressive structural failure and a loss of façade integrity. For specimens 2 and 3, their temperatures are comparable to those of specimen 1 at heights ≤ 0.9 m but significantly lower at heights ≥ 1.5 m. This suggests that while the façades of specimens 2 and 3 are burned out at heights ≤ 0.9 m, they maintain structural integrity at heights ≥ 1.5 m. These results underscore the enhanced fire performance of specimens 2 and 3, achieved through fire-retardant treatment, which effectively limits flame spread beyond the direct impact of outflow flames and restricts flame heating within the vent layer.

In Figure 6, the left side shows flame morphologies of specimens 1–3 at 140 and 860 s, corresponding to the time of temperature peaks in specimen 1. Combined with the flame morphology during the calibration test, it becomes evident that the fire-retardant-treated cedar contributes minimally to façade flame spread. Conversely, specimen 1 exhibits pronounced flame spread, with higher flame tips reaching the façade top during both initial and secondary combustion. As previously discussed, the intensified flame spread is attributed to surface layer combustion and vent layer flame penetration, both of which can be observed in the upper part of the façade through heavy soot production. In this case, the visible flame heights are elongated significantly compared to the fire-retardant-treated cedar specimens.

The qualitative comparison of façade burnt areas after the JIS A 1310 tests is illustrated in Figure 7a. It is evident that the burnt area of specimen 1 is significantly larger than that of specimens 2 and 3. Notably, specimen 1 exhibits narrower charred edges, with its burnt area comparable to the charred areas in specimens 2 and 3. This indicates that the thermal attack region of outflow flames promotes flame spread along untreated cedar but is restricted to surface char formation in fire-retardant-treated cedar. The burnt areas in specimens 2 and 3 are comparable to the non-soot area above the opening formed in the calibration test. This can be attributed to the complete re-mixing of outflow fuel with air near the opening, resulting in a luminous flame with higher temperatures. Consequently, the cedar façades, even those treated with fire retardant, become fully charred under direct flame impact, ultimately losing their mechanical properties and burning out.

According to the zoomed post-combustion observation near the opening in Figure 7b, specimens 2 and 3 exhibit a smaller burnt area and a larger charred area compared to specimen 1. Additionally, exudation of fire retardant is found on the surface of specimens 2 and 3, suggesting that the high-pressure impregnated fire retardant migrates to the cedar surface under the intense thermal impact of the flame. Note that this exudation behavior is less pronounced in specimen 3, which can be attributed to accelerated weathering that leaches out fire retardant and reduces its retention, thereby limiting surface exudation. The leaching effect in cedar is caused by water penetration into the cell lumina and tracheids, where the fire retardants are deposited [18]. In this case, the fire retardants diffuse gradually toward the surface along the continuous water pathways. Driven by concentration gradients, this leaching process originates at the surface and progressively extends inward with prolonged weathering [19]. Nevertheless, the leaching effect has a minor

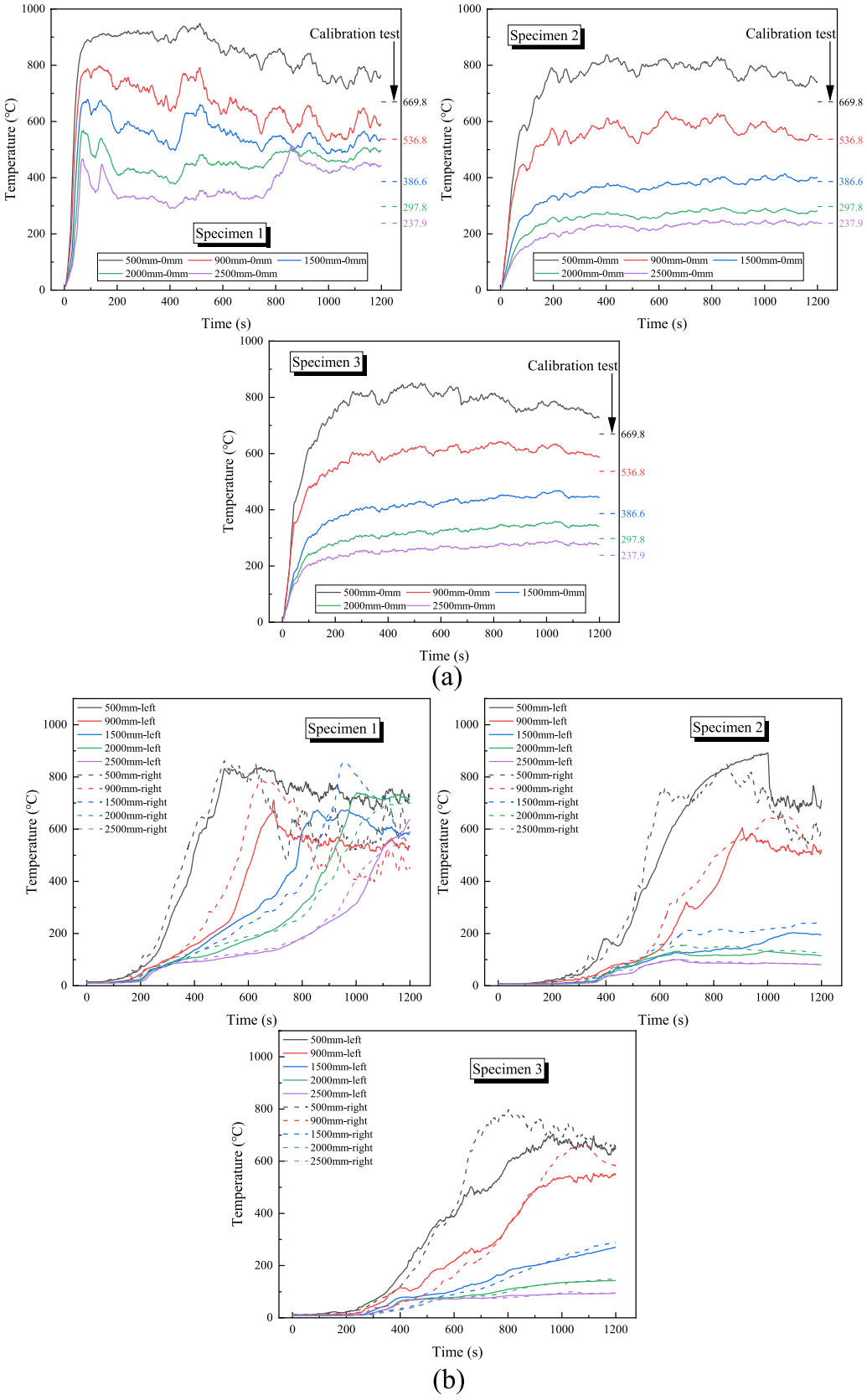

FIGURE 5 | Temperature histories of specimens 1, 2, and 3. (a) Temperature along the façade surface. (b) Temperature inside the vent layer.

contribution to the flame spread of fire-retardant cedar owing to the presence of alkyd coating; even after accelerated weathering, its fire performance remains stable, indicating superior weathering resistance and minimal degradation.

3.2 | Modeling of Cedar Façade Fire

As shown in Figure 8, the flame temperature along the cedar façade is compared between modeling and experiments. This

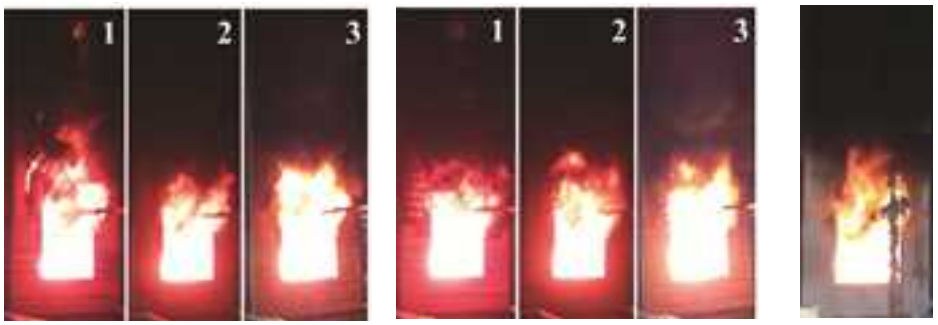

FIGURE 6 | Flame morphologies of specimens 1–3, and calibration test.

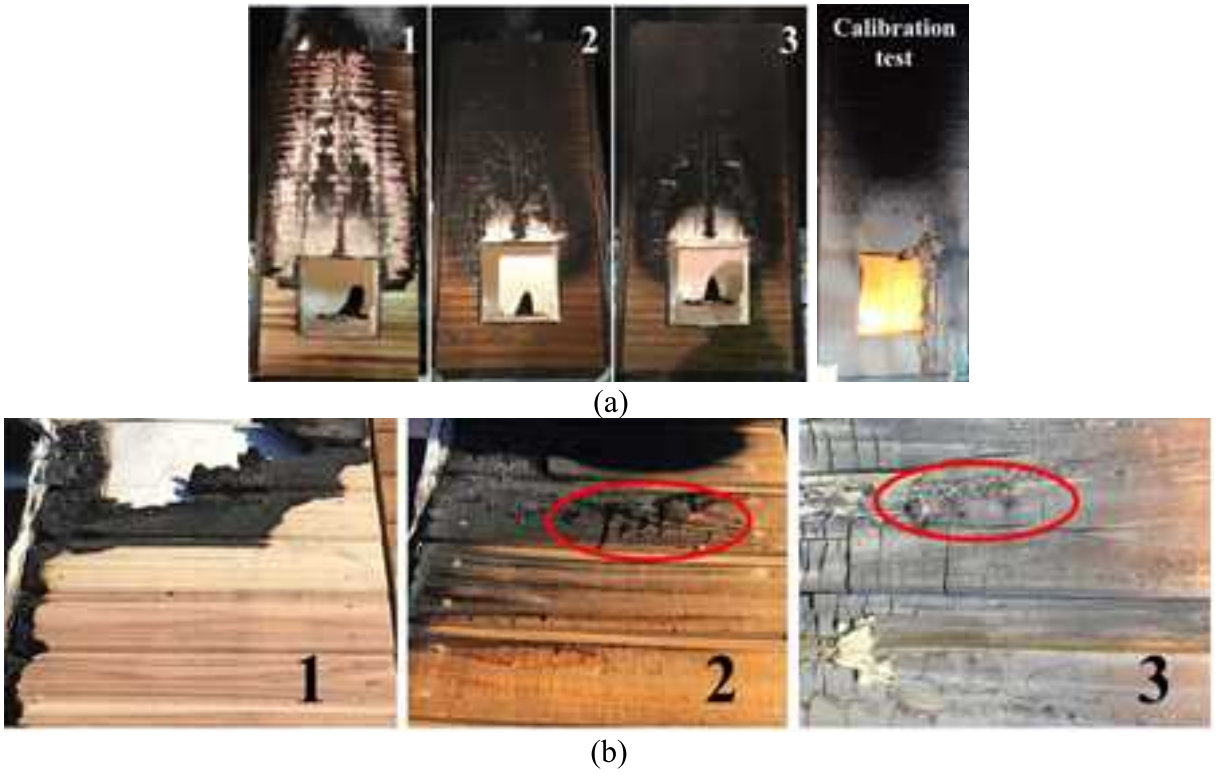

FIGURE 7 | Appearance of specimens 1–3 and calibration test after experiment. (a) Front view. (b) Regions near the vertical edge of the opening.

validation is based on the experimental temperatures of specimen 1, that is, cedar façade without fire retardant treatment or accelerated weathering, which features significant flame spread. The modeling successfully captures the initial temperature peak induced by surface combustion. Generally, good agreement is achieved in the modeling for heights up to 1500 mm. However, at heights exceeding 2000 mm and beyond 900 s, the modeled temperatures are lower than the experimental results due to physical structure breakdown (i.e., cedar panel below 1500 mm height is burned away), which is not involved in the current modeling. In the experimental analysis, the broken cedar façade leads to flame penetration into the vent layer and subsequent spread along the back of the façade. However, in the modeling, the flame is only imposed on the front of the façade (the backward is considered a constant convection heat transfer without the modeling of the vent layer), thus resulting in the absence of the second temperature peak attributed to back heating. On the other hand, at heights below 1500 mm, where the direct impact of outflow flames, combustion takes place at the front side of the façade, and the cedar panels burn out rapidly, leading to better agreement between modeling and experiments. Consistent with the temperature trend of the flat cedar façade fire, the modeled temperatures at all heights are higher than those in the calibration test, with more pronounced increases at higher positions.

The flame morphology obtained by the modeling and video camera is presented in Figure 9. In this case, the flame morphology in modeling is defined by the temperature of 540°C [20]. To reduce uncertainty, the modeled temperature is averaged over each 5-s interval to capture the overall trend of flame morphology. During the experiment, rapid charring of the cedar is observed shortly after the flame attaches to the façade surface, as well as on both sides of the opening. As the test progresses, the cedar directly exposed to the outflowing flame undergoes rapid failure, after which the burned-out area gradually expands upward as the flame spreads. In the modeling, the overall evolution

of the flame is captured, showing a gradual decline over time. The modeling shows rapid flame spread within the first 200 s, consistent with experimental observations, though partially obscured by soot. This suggests that the formation of char layers is the major factor in limiting further flame spread along the cedar surface.

With respect to the burnt area, the modeling is compared to the experiment in Figure 10. The burnt area is determined by the percentage of cedar in each cell. The transition from cedar to char is implemented based on the pyrolysis modeling, characterized by reaction parameters shown in Table 2. Under flame impingement, cedar cells gradually convert to char cells, with a decreasing cell cedar percentage. The char cells adjacent to the high-temperature region act as a thermal barrier, limiting further pyrolysis of the deeper cedar façade. Combined with the experimental result, areas where the cedar percentage is lower than 0.5 are designated as the burnt area, showing reasonably good agreement with the experiment. The burnt area in the experiment is relatively larger compared to the modeling, extending both vertically and horizontally. For this discrepancy, in addition to the reason for flame penetration into and subsequent spread within the vent layer, another contributing factor could be the horizontally assembled cedar panels, which facilitate flame spread along the joints between each panel.

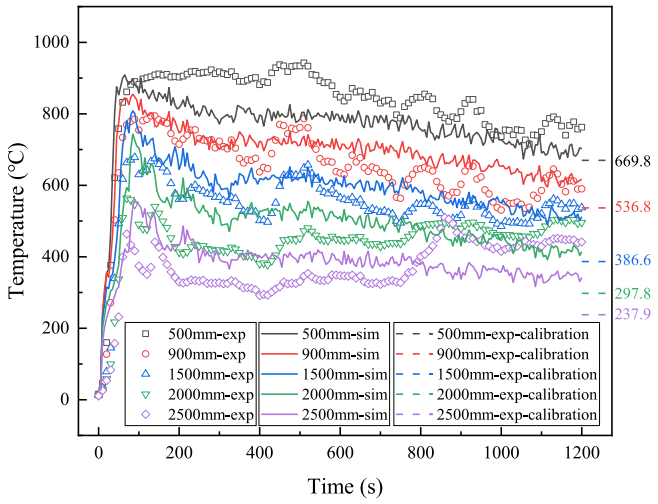

FIGURE 8 | Façade temperature comparisons for specimen 1 (no fire retardant or accelerated weathering) between experiment and modeling.

FIGURE 10 | Comparison of burnt area after test between experiments and modeling.

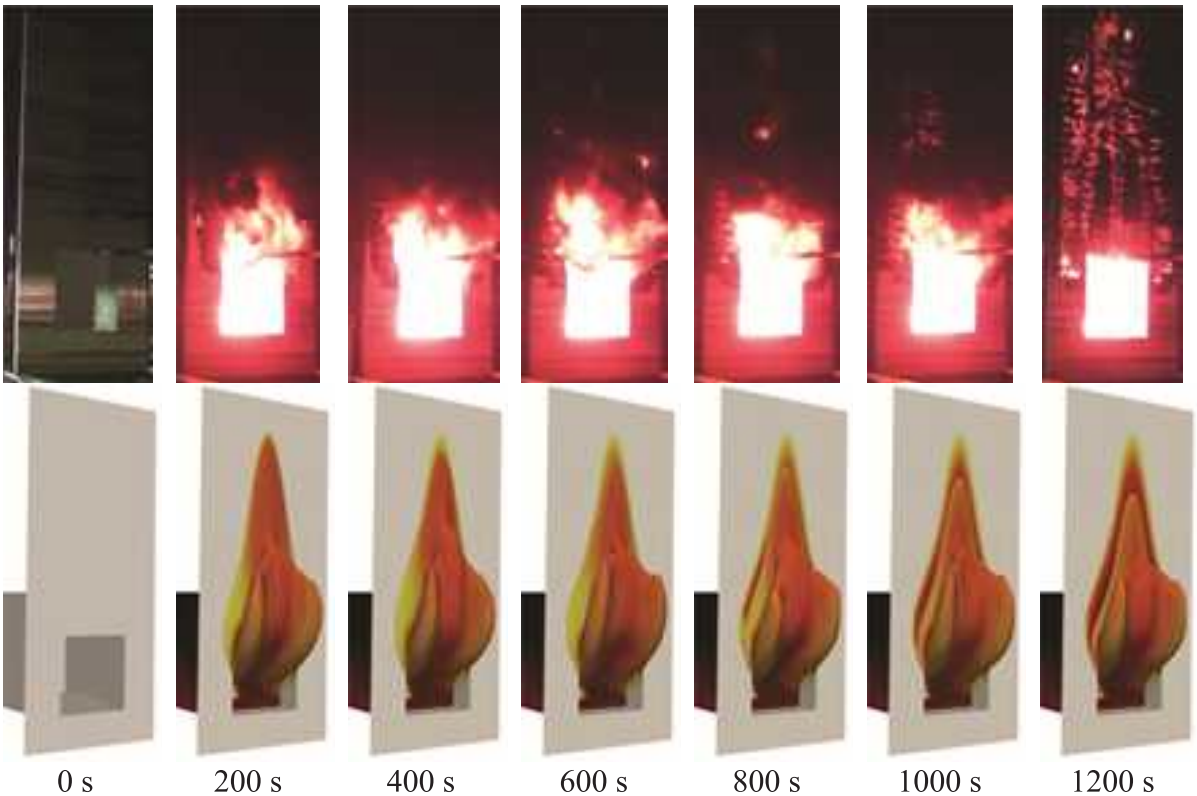

FIGURE 9 | Flame spread of experiment and modeling at varied times.

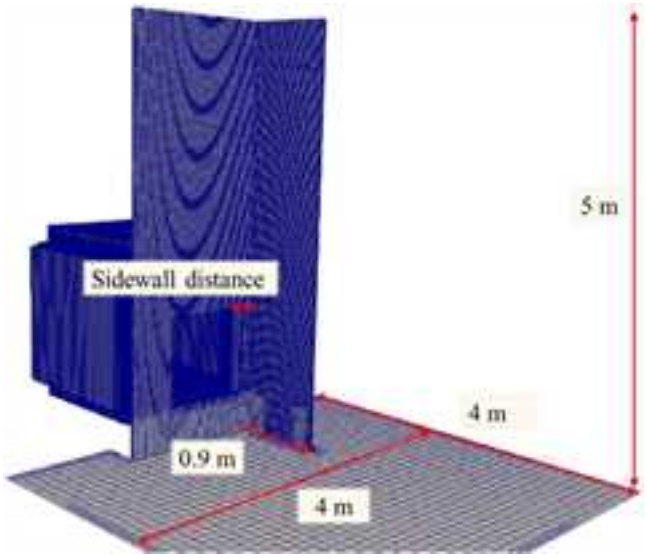

FIGURE 11 | Computational domain of cedar façade with 0.1 m sidewall distance.

3.3 | Sidewall Effect on Cedar Façade Fire

Sidewall cedar façade fires are investigated based on this validated numerical configuration, with a single sidewall ($L \times W \times H = 0.9\,\text{m} \times 0.05\,\text{m} \times 4.1\,\text{m}$) located adjacent to the opening, as shown in Figure 11. Here, sidewall distances, defined as the distance between the opening and the sidewall, ranging from 0.1 to 0.3 m, are considered. The sidewall configurations are identical to those of the main façade wall, adopting the same cedar properties and vent layer assumption.

Figure 12 presents flame spreads of different sidewall distances and no sidewall, with the flame morphology determined by the temperature of 540°C [20] (based on the temperature averaged over each 5-s interval). This figure showcases the flame morphology when the burnt area reaches the façade top. For the cedar façade fire without the sidewall, the flame morphology at the end of the test (1200 s) is presented since it has not spread to the façade top during the whole test duration. Generally, the flame spread is accelerated at smaller sidewall distances due to limited

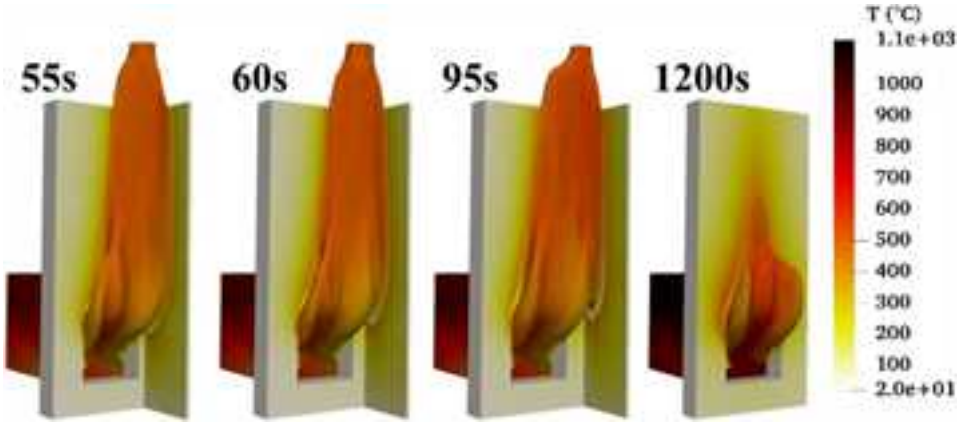

FIGURE 12 | Flame morphology of specimen 1 (no fire retardant or accelerated weathering) varying sidewall distance (left to right: 0.1–0.3 m and no sidewall).

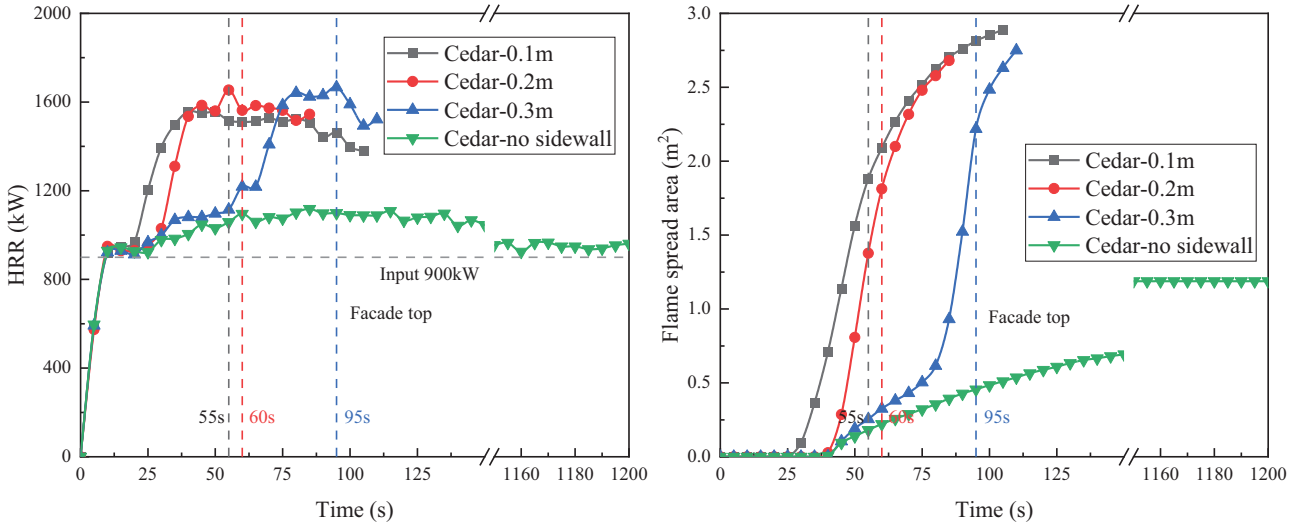

FIGURE 13 | Histories of HRR and burnt area with different sidewall distances.

air entrainment and elongated fuel combustion along the sidewall corner. In flat cedar façades, the thermal attack from outflow flame reattachment is limited, leading to relatively lower flame heights and mitigated cedar combustion. However, in the presence of sidewalls, intensive flame attachment coupled with enhanced thermal attack at the sidewall corner results in a larger area of cedar combustion. In this scenario, the restricted air entrainment further transports a large amount of volatiles to elevated positions, thereby significantly accelerating the flame spread.

The developments of HRR and burnt area are illustrated in Figure 13 for sidewall distances of 0.1–0.3 m and for a flat cedar façade without sidewalls. Except for the flat cedar façade, each case is terminated shortly after the burnt area reaches the façade top, with dashed lines marking the timing of this occurrence. Generally, the HRR is the direct indicator related to the fire risk of cedar façades. The flat cedar façade exhibits the lowest fire risk, with a peak HRR below 1200 kW and a flame burnt area approaching the plateau of 1.2 m^2. In this case, the HRR contribution from cedar combustion peaks at around 220 kW. Conversely, sidewall cedar façades, irrespective of sidewall distance, demonstrate a significantly higher fire risk, with peak HRRs reaching approximately 1670 kW. Here, the HRR contribution from cedar combustion in sidewall conditions is 3.5 times greater than that of the flat façade. While peak HRRs are comparable among sidewall cedar façades, increasing the sidewall distance effectively delays flame spread. In our previous work [4, 21], a sidewall distance of $\geq$0.2 m is identified as a threshold to mitigate thermal attack and reduce the fire risk of sidewall façades (non-combustible). However, due to the intensive façade flame accumulation at the sidewall corner caused by cedar combustion, the 0.2 m sidewall distance shows a similar flame spread to that of the 0.1 m sidewall distance, with a pronounced 35-s delay between the 0.2 and 0.3 m sidewall distances. This indicates that when considering cedar façades, the fire-risky sidewall distance is enlarged by additional HRR from material combustion.

4 | Conclusion

In this study, the flame spread along large-scale cedar façades is investigated experimentally and numerically based on the JIS A 1310 test, with analyses focusing on the effects of fire retardant treatments, accelerated weathering, and sidewall effect on cedar fire behavior. The following conclusions are obtained:

1. For the untreated cedar specimen, flame spread within the vent layer plays a critical role, contributing to thermal attacks on both the front and back of the cedar façade. This process leads to secondary combustion in regions beyond the direct impact of outflow flames. The fire-retardant-treated cedar demonstrates good fire performance. Even after the leaching effect caused by accelerated weathering in accordance with JIS A 1326, its fire performance shows limited deterioration and remains substantially more effective than that of the untreated cedar.
2. The modeling of flame spread along the cedar façade shows good qualitative agreement with experimental data. However, discrepancies arise in the underestimation of the secondary peak in façade temperatures, which is attributed to the simplified assumptions without incorporating the vent layer flame spread.
3. Modeling of sidewall cedar façade fires reveals that the presence of sidewalls significantly elevates fire risk, with accelerated flame spread occurring at smaller sidewall distances. Additionally, the results indicate that the additional HRR from cedar façade combustion tends to enlarge the fire-risky sidewall distance.

Acknowledgments

The authors gratefully acknowledge the helpful discussions with Drs. Yi Wang, Ning Ren, Xiaoyi Lu, and Gaurav Agarwal from FM Global, as well as the cedar samples provided by Koshii & Co. Ltd. This work was partially supported by the project of Japan Society for the Promotion of Science (Grant Number 22KK0062).

Funding

This work was supported by Japan Society for the Promotion of Science (Grant Number 22KK0062).

Conflicts of Interest

The authors declare no conflicts of interest.

Data Availability Statement

The data that support the findings of this study are available from the corresponding author upon reasonable request.

References

1. M. P. Giraldo, J. Avellaneda, A. Lacasta, and C. Burgos, "Numerical-Simulation Research on Building-Façade Geometry and Its Effect on Fire Propagation in Wooden Façades," *World Conference on Timber Engineering* (2014): 1–8.

2. T. Engel and N. Werther, "Structural Means for Fire-Safe Wooden Façade Design," *Fire Technology* 59 (2023): 117–151.

3. E. Guillaume, V. Drean, B. Girardin, F. Benameur, M. Koohkan, and T. Fateh, "Reconstruction of Grenfell Tower Fire. Part 3—Numerical Simulation of the Grenfell Tower Disaster: Contribution to the Understanding of the Fire Propagation and Behaviour During the Vertical Fire Spread," *Fire and Materials* 44, no. 1 (2020): 35–57.

4. X. Sun, H. Yoshioka, T. Noguchi, et al., "Large Eddy Simulations Fire Modeling of JIS A 1310 Façade Calibration Test With Respect to Sidewall," *Fire and Materials* 48, no. 4 (2024): 411–425.

5. D. Dhima, M. Duny, J.-P. Garo, H.-Y. Wang, and Q. Jullien, "Experimental Study on Vertical Wooden Façade Combustion," *Procedia Engineering* 210 (2017): 520–527.

6. B. Östman and L. Tsantaridis, "Fire Scenarios for Multi-Storey Façades With Emphasis on Full-Scale Testing of Wooden Façades," *Fire Technology* 51 (2015): 1495–1510.

7. T. Hakkarainen and T. Oksanen, "Fire Safety Assessment of Wooden Facades," *Fire and Materials* 26, no. 1 (2002): 7–27.

8. Y. Nishio, H. Yoshioka, T. Noguchi, et al., "Fire Spread Caused by Combustible Facades in Japan," *Fire Technology* 52 (2016): 1081–1106.

9. M. Duny, D. Dhima, H.-Y. Wang, J.-P. Garo, and B. Manescau, "Impact of Façade Type on an Ejected Flame Propagation From a Compartment Opening-Experimental and Numerical Studies," *Journal of Building Engineering* 46 (2022): 103660.

10. B. Zhou, H. Yoshioka, M. Kanematsu, and T. Noguchi, "Numerical and Experimental Study of Cedar Façade Fire," *Fire and Materials* 46, no. 2 (2022): 476–486.

11. JIS A 1310 Standard Test, *Test Method for Fire Propagation Over Building Facades* (Japanese Standards Association, 2015).

12. JIS C 1602, *Thermocouple* (Japanese Standards Association, 1995).

13. JIS Z 8703, *Standard Atmospheric Conditions for Testing* (Japanese Standards Association, 1983).

14. JIS A 1326:2019, *Test Method for Accelerated Weathering of Fire-Retardant Treated Wood Products for Façades* (Japanese Standards Association, 2019).

15. N. Ren and Y. Wang, "A Convective Heat Transfer Model for LES Fire Modeling," *Proceedings of the Combustion Institute* 38, no. 3 (2021): 4535–4542.

16. fireFoam-dev, https://github.com/fireFoam-dev.

17. N. Ren, J. de Vries, X. Zhou, M. Chaos, K. V. Meredith, and Y. Wang, "Large-Scale Fire Suppression Modeling of Corrugated Cardboard Boxes on Wood Pallets in Rack-Storage Configurations," *Fire Safety Journal* 91 (2017): 695–704.

18. T. Harada, H. Matsunaga, Y. Kataoka, M. Kiguchi, and J. Matsumura, "Weatherability and Combustibility of Fire-Retardant-Impregnated Wood After Accelerated Weathering Tests," *Journal of Wood Science* 55 (2009): 359–366.

19. R. H. White, *Accelerated Weathering of Fire-Retardant-Treated Wood for Fire Testing* (BCC Research, 2009), 246–256.

20. L. Seigel, "The Projection of Flames From Burning Buildings," *Fire Technology* 5 (1969): 43–51.

21. X. Sun, H. Yoshioka, T. Noguchi, Y. Nishio, T. Hayakawa, and B. Zhou, "Experimental and Numerical Investigation of Façade Flame With Respect to Varied Distances Between Sidewall and Main Wall Opening," *Thermal Science and Engineering Progress* 54 (2024): 102842.